MOLECULAR CLOUDS IN THE CARINA ARM: THE LARGEST OBJECTS; ASSOCIATED REGIONS OF STAR FORMATION; AND THE CARINA ARM IN THE GALAXY

D. A. GRABELSKY,[1] R. S. COHEN,[1] L. BRONFMAN,[1,2] AND P. THADDEUS[1,3,4]

ABSTRACT

The Columbia CO survey of the southern Galactic plane is used to identify giant molecular clouds and cloud complexes in the Vela-Carina-Centaurus section of the Milky Way. Twenty-seven giant molecular clouds between $l = 270°$ and $300°$ are cataloged and their heliocentric distances given. In addition, 16 clouds at $l > 300°$ beyond the solar circle extend the catalog to include the very distant portion of the Carina arm. The most massive clouds in the catalog ($M \geq 10^5 \, M_\odot$) trace the Carina arm over 23 kpc in the plane of the Galaxy. The average mass of these objects is $1.4 \times 10^6 \, M_\odot$, and their average spacing along the arm is 700 pc. The composite distribution projected onto the Galactic plane of the largest molecular clouds in the Carina arm and of similarly massive clouds in the first and second quadrants strongly suggests that the Carina and Sagittarius arms form a single spiral arm ~ 40 kpc in length wrapping two-thirds of the way around the Galaxy. Descriptions of each cloud, including identification of associated star-forming regions, are presented in an Appendix.

Subject headings: galaxies: structure — galaxies: The Galaxy — interstellar: molecules

I. INTRODUCTION

More than 2–3 kpc from the Sun, optical tracers of spiral arms are generally obscured, and the study of large-scale Galactic structure has relied mainly on radio spectral-line observations. Historically, the various models of the Galaxy's spiral arms offered by radio observations have not been fully consistent either with each other or with the extrapolation of optical spiral structure (e.g., Kerr 1970; Weaver 1970; Georgelin and Georgelin 1976). An outstanding exception to the veil of extinction that sets in beyond the local optical arms is found in the Carina region of the Milky Way where the Carina arm is traced in all Population I objects, radio *and* optical, over distances of 2–10 kpc and beyond. The first demonstration that giant molecular clouds are good tracers of the Carina arm was given by Cohen et al. (1985) on the basis of early results from the Columbia CO survey of the southern Milky Way. In a more recent paper (Grabelsky et al. 1987, hereafter Paper I) we amplified this analysis, providing details on the observations and expanding the discussion of the distribution of molecular clouds in and around the arm.

We concentrated in Paper I on the large-scale description of the Carina arm, showing that it is one of the clearest examples of Galactic CO spiral structure, with an arm-interarm contrast in molecular clouds of at least 10:1, and comparing in some detail the distributions of CO and H I in the outer Galaxy. Determination of the molecular cloud distribution in the Galactic plane and the possible resolution of the long-standing problem of connecting the Carina arm to the arms in the northern Milky Way (e.g., Simonson 1979; Henderson, Jackson, and Kerr 1982) was deferred. We address these tasks in the present paper by cataloging the largest individual molecular clouds in our survey and identifying their associated star-forming regions, and then piecing together the Galactic plane

distribution of the Carina-arm clouds with that of the largest clouds identified in the Columbia CO surveys of the northern Milky Way.

The problem of definition and identification of giant molecular clouds is somewhat analogous to that of OB associations (see Blaauw 1964): the larger stellar associations often contain distinct subgroups, occupy large volumes of space, and are fairly conspicuous, whereas the smaller ones are often hard to distinguish from the field stars. The outer boundary of an association, where member stars blend in with the field, is generally poorly defined, even when there is little doubt that the association exists. Similarly, giant molecular clouds are typically complexes of smaller clouds, can occupy 10^6 pc^3, and, even across the Galaxy, stand out fairly prominently against the background of smaller molecular clouds. Examples of nearby, fairly isolated giant clouds, such as those associated with Cas A and NGC 7538 in the Perseus arm (Dame et al. 1986), indicate that the largest ones have masses well in excess of $10^6 \, M_\odot$, linear extents of 50–100 pc, and internal velocity dispersions of 10–20 km s^{-1}. Although the boundaries of these very large complexes are also often difficult to define, the local examples leave little doubt as to their existence. The ability to resolve each individual cloud within a complex is largely irrelevant to the task of detecting the complex as a whole above the background; very high angular resolution is often not required and can be a liability if it leads to undersampling.

This loose analogy with OB associations does not extend to the overall mass distribution: unlike OB associations, which collectively represent only a small fraction of the total stellar mass of the Galaxy, the largest molecular clouds apparently contain most of the molecular gas content of the Galaxy, with $\sim 85\%$ of the mass in clouds more massive than $10^5 \, M_\odot$ (Dame et al. 1986). Our discussion is focused on the largest molecular clouds in the Carina arm.

The significance of giant molecular clouds as tracers of Galactic spiral structure, although suspected almost as early as their discovery (e.g., Schwartz, Wilson, and Epstein 1973), has become clear only recently and owes its recognition largely to

[1] Columbia University.
[2] Universidad de Chile.
[3] Goddard Institute for Space Studies.
[4] Harvard-Smithsonian Center for Astrophysics.

extensive, well-sampled CO surveys made with the Columbia Northern and Southern Millimeter-Wave Telescopes. As the study of molecular clouds associated with nearby star-forming regions, such as that in Orion, began to provide evidence for the existence of large molecular cloud complexes (e.g., Tucker, Kutner, and Thaddeus 1973; Kutner *et al.* 1977), the possibility was raised that such clouds, represented by the local examples, are common throughout the Galaxy. Closely associated with Population I material, they were obvious candidates for spiral arm tracers. With masses of $10^6 M_\odot$ or greater (e.g., Elmegreen and Lada 1976; Dame 1983), they also clearly rank among the most massive objects in the Galaxy.

Indirect evidence from early Galactic CO surveys suggested that perhaps as much as 50% of the total mass of molecular clouds in the Galaxy resided in clouds more massive than $10^6 M_\odot$ (e.g., Solomon, Saunders, and Scoville 1979), but the severe undersampling of the early surveys (a constraint imposed by overresolution) essentially dissected most of these giant clouds. As *distinct* objects they went largely unrecognized, and their distribution projected onto the Galactic plane remained an open question. By 1980, CO surveys undertaken with the Columbia Northern Telescope provided sufficient coverage and sampling of the first and second quadrants to reveal a string of very large molecular clouds that trace the Perseus arm, as well as to identify the molecular counterparts of the classic inner-Galaxy 21 cm arms (Cohen *et al.* 1980). Completion of these surveys made possible a systematic search for distinct cloud complexes in the inner Galaxy and study of their distribution on a Galactic scale. With the Columbia CO survey of the first quadrant, Dame (1983) (also see Dame *et al.* 1986) identified 25 molecular cloud complexes more massive than $5 \times 10^5 M_\odot$, including 13 more massive than $10^6 M_\odot$. These objects were generally found to lie along spiral arms and even at very great distances to stand out fairly clearly in the data.

The approach of Dame *et al.*, which we adopt here, is essentially the conventional one: to assume that the properties of a class of objects observed locally can be used to study similar objects at great distance. Here, the Carina-arm clouds are shown not only to be generally associated with known star-forming regions but also, when projected onto the plane of the Galaxy, to trace the continuation into the fourth quadrant of the Sagittarius arm in the first. In giant molecular clouds, the Carina-Sagittarius arm stretches more than 40 kpc around the Galaxy. As an exhibit of the value of CO in tracing the large-scale structure of the Galaxy it is unsurpassed.

A summary of the observations is given in § II. In § III the general procedure for identifying clouds in the survey and locating them in projection on the Galactic plane is described, with the large cloud associated with the η Carinae nebula as an example. The completeness of the cloud catalog is then briefly considered. In the discussion in § IV, 43 molecular clouds identified between $l = 270°$ and $336°$ generally more massive than

$10^5 M_\odot$ are used to trace the Carina arm in the plane of the Galaxy, and the implications for large-scale Galactic structure are emphasized. Our conclusions are given in § V. The Appendix provides a brief description of each cloud in the catalog, including specific criteria for definition and identification of associated stars and star-forming regions.

As in Paper I, here the *old* values of Galactic constants R_0 and V_0 (10 kpc and 250 km s^{-1}) are used to facilitate comparison with published results of previous Galactic surveys. The effect on our results of adopting the new values of R_0 and V_0 recently recommended by the IAU (8.5 kpc and 220 km s^{-1}; see Kerr and Lynden-Bell 1986) are discussed in the Appendix to Paper I.

II. OBSERVATIONS

The observations were made between 1983 January and November with the Columbia Southern Millimeter-Wave Telescope at Cerro Tololo, or the Chile Telescope for short, a close copy of the Columbia Northern Millimeter-Wave Telescope, or the New York Telescope. A detailed discussion of the observations and instrumentation is given in Paper I (see also Grabelsky 1985; Bronfman 1986). Table 1 summarizes the most important parameters of the Chile antenna, receiver, and spectrometer at the time of the observations. The receiver was calibrated with a standard blackbody chopper-wheel, and the resultant antenna temperatures, corrected for atmospheric losses, were adjusted slightly ($\sim 10\%$) to agree with the temperature scale of the New York Telescope (Bronfman *et al.* 1987). Line intensities here are antenna temperatures corrected for atmospheric attenuation and main-beam efficiency and are approximately equal to the effective radiation temperature, T_R, for a source that just fills the main beam.

Observations were made by position switching against reference positions verified to be free of CO emission. To assure flat baselines, the difference in elevation between source and reference positions was generally kept to less than 0°.5. Integration times were typically 5 minutes, yielding an rms noise per channel of ~ 0.14 K. After subtraction of a linear baseline from each spectrum, occasional spectra with baseline curvature greater than twice the rms were rejected and the positions reobserved.

Two concurrent surveys of the Carina region were carried out, each extending from $l = 270°$ to $300°$ and covering 333 km s^{-1} (centered at $v_{LSR} = 0$) with a spectral resolution of 1.3 km s^{-1}, but differing in latitude coverage and spatial resolution. The main or full-resolution survey covered $|b| \leq 1°$, with some latitude extensions at $l = 280°$ (the tangent direction of the Carina arm); sampling was every 0°.125 in l and b, i.e., slightly better than one beamwidth (0°.147). The companion low-resolution survey covered $|b| \leq 5°$ at a spatial resolution of 0°.5, with a sampling interval of 0°.5 in l and b (see Paper I). Where the Carina arm extends beyond $l = 300°$, observations

TABLE 1

PROPERTIES OF THE CHILE TELESCOPE

Antenna	1.2 m Cassegrain
Beamwidth (FWHM)	8′.8
Pointing accuracy	<1′
Receiver	LN2 cooled Schottky barrier diode mixer
Noise temperature	385 K
Spectrometer	256 channel filterbank
Resolution	0.5 MHz per channel (1.3 km s^{-1} at 115 GHz)
Bandwidth	333 km s^{-1} at 115 GHz

from a third, adjoining survey (Bronfman 1986) carried out on the same telescope are used.

The l, v map of most of the fourth quadrant presented in Paper I is relevant to the present discussion and is reproduced here in Figure 1. Its salient feature is the open loop formed by segments at negative velocity from $l \approx 280°$ to $300°$ and positive velocity at $l \geq 280°$, joined by the intense emission centered at $v \approx 0$ km s^{-1} near $l = 280°$. This loop is the Carina

arm, that part at negative velocity originating from the near side, that at positive velocity from the far side, and that near zero velocity from the tangent point. The kinematic interpretation of this loop is discussed in Paper I.

III. IDENTIFICATION OF CARINA-ARM CLOUDS

In CO, the loop of the Carina arm in the l, v diagram (Fig. 1) is not characterized by a generally continuous lane of emission,
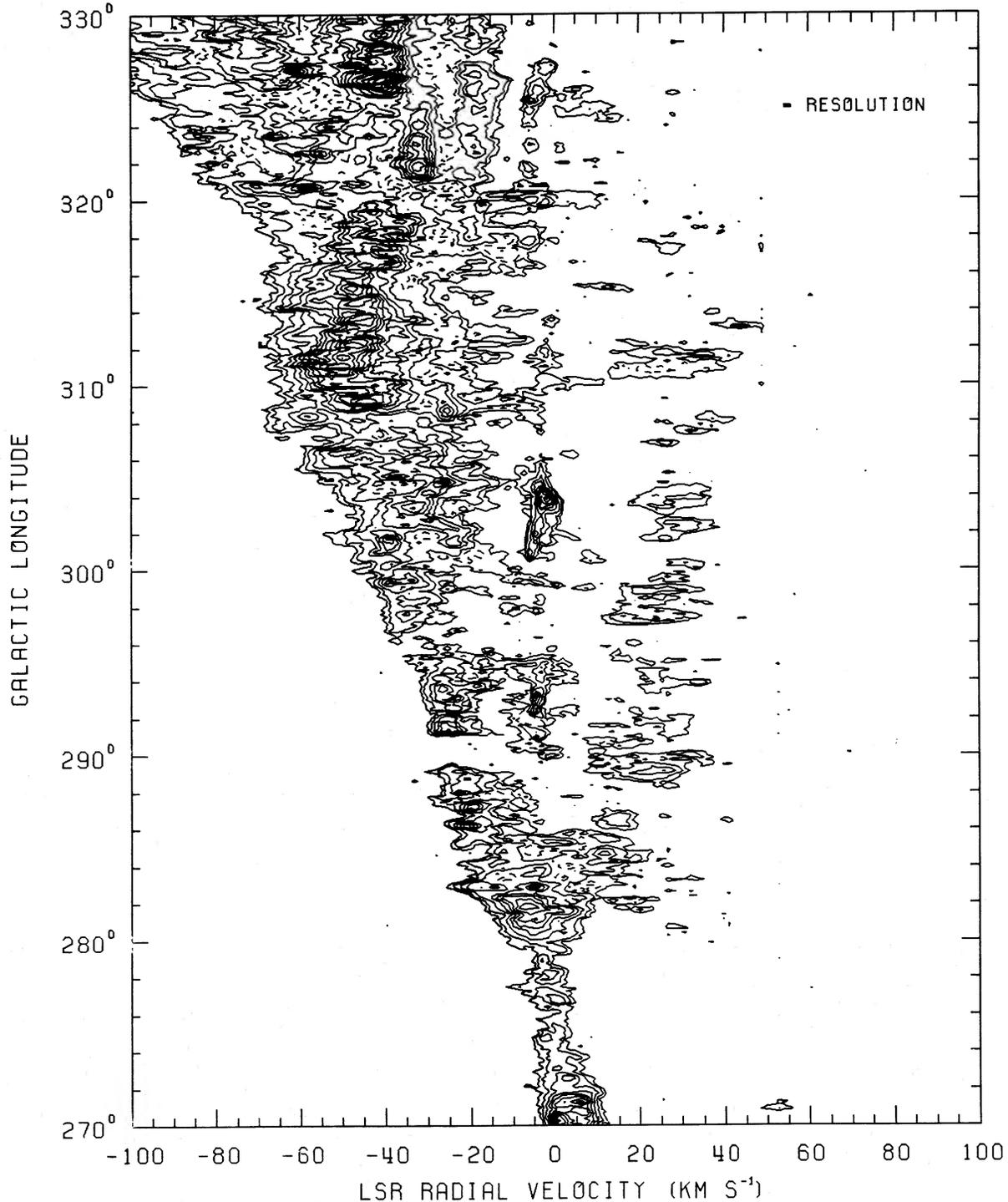

FIG. 1.—Longitude-velocity diagram for the full-resolution (0°125) CO survey. The CO emission has been integrated over all latitudes where data were taken (see Paper I for details). Contours are at 0.35, 0.7, 1.4, 2.1, ... K deg.

NEAR SIDE: V =   -50 TO   -9 KM S⁻¹

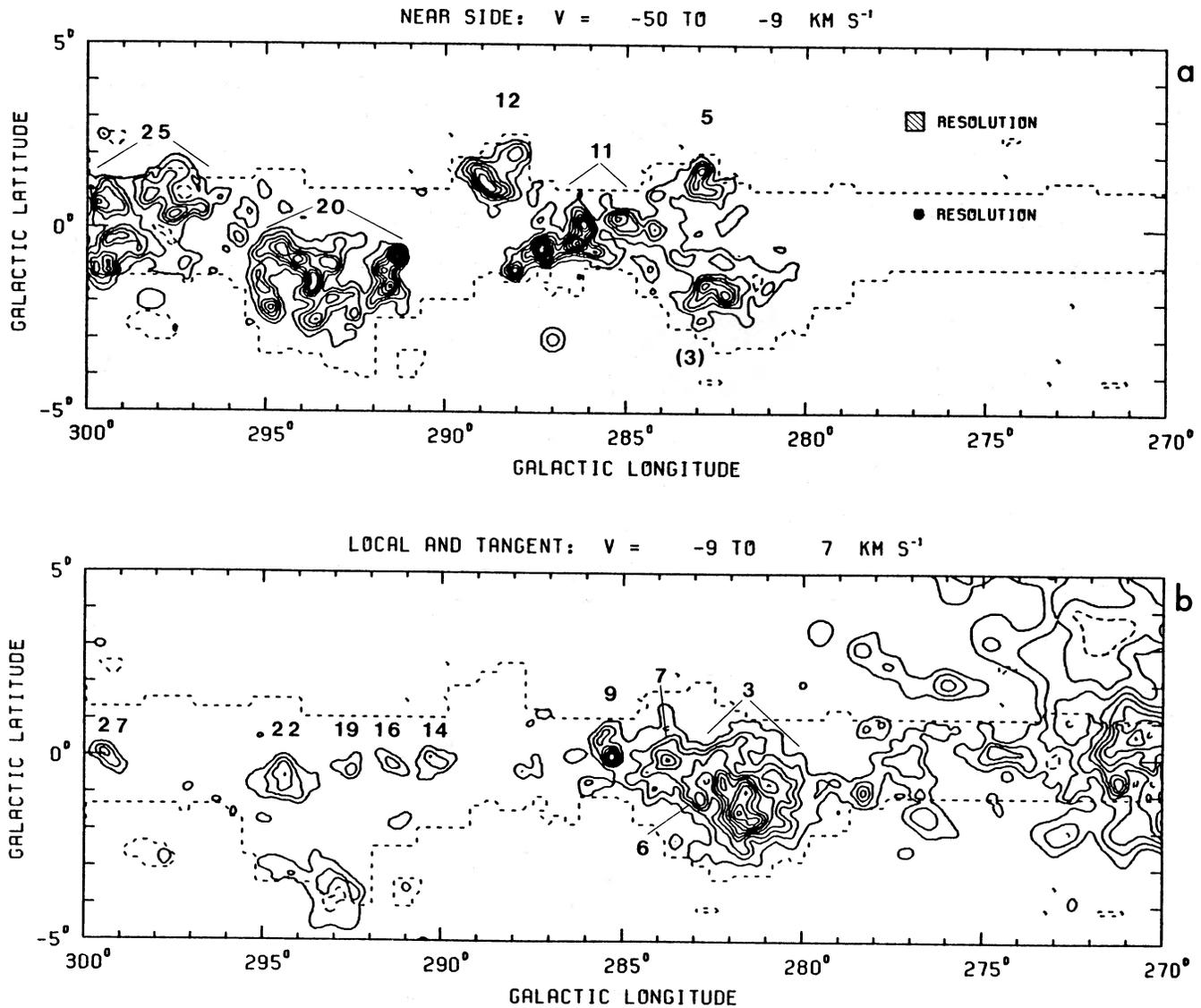LOCAL AND TANGENT: V =   -9 TO   7 KM S⁻¹

FIG. 2.—Spatial maps of CO emission integrated over the indicated velocity ranges: (a) the near side of the Carina arm, (b) the tangent region, and (c) and (d) the far side. Inside the dotted lines in the maps covering $l = 270°$ to $300°$ (a–c) and at $l > 300°$ (d), full-resolution data are shown smoothed to $0°.25$ resolution. Beyond the dotted lines in parts (a)–(c), where low-resolution ($0°.5$) data are shown, the spectra are "clipped," i.e., all spectral channels with $T < 0.5$ K were set to zero before integration. The contour interval is 3 K km s⁻¹. The numbers in boldface identifying the molecular clouds in the survey correspond to the running numbers in Table 2. For extended clouds, a pair of lines radiating from the number indicates the cloud's extent; where the identification may appear ambiguous, a single line from the number points to the cloud. A pair of numbers separated by a comma indicates that clouds with nearly the same spatial coordinates have been blended in velocity by the integration. The parenthetical "3" in the near side map (a) refers to emission from cloud no. 3 that extends across the velocity boundary between the tangent region map (b) and the near side map.

as it is in H I, but instead by a chain of several dozen discrete objects: the molecular clouds. These clouds are similar in appearance to the largest molecular clouds in the first and second quadrants, with velocity widths of ~10 km s⁻¹ and linear sizes of ~100 pc. Some clouds, particularly in the far side of the arm, are well defined in longitude and velocity. In the near side of the arm, groups of peaks, for example between $l = 291°$ and $296°$, were classified as cloud complexes if they could be shown to be at the same distance, e.g., by association with optical objects with known distances. Identification of individual giant molecular clouds in the highly blended tangent region is quite ambiguous. A preliminary list of molecular clouds in the Carina arm was compiled from these identifications in the l, v diagram. Clouds interior to the loop (i.e., near

zero velocity), except those clearly local, were also included on the preliminary list.

This list was checked against identifications made with the spatial maps, shown in Paper I, of emission in the near side, tangent region, and far side of the Carina arm. Those maps were spatially smoothed to $0°.25$ to produce the spatial maps shown here in Figure 2. The smoothed maps provide a higher signal-to-noise ratio and highlight large clouds in the near side. Generally, the same clouds and cloud complexes were identified in both the l, v diagram and the spatial maps, adding confidence to the assignments. In a few cases, the spatial maps showed that separate clouds at the same longitude had been blended in the l, v map as a result of the integration in latitude. For example, at $l \approx 283°$, two separate objects at $b = +1°$ and

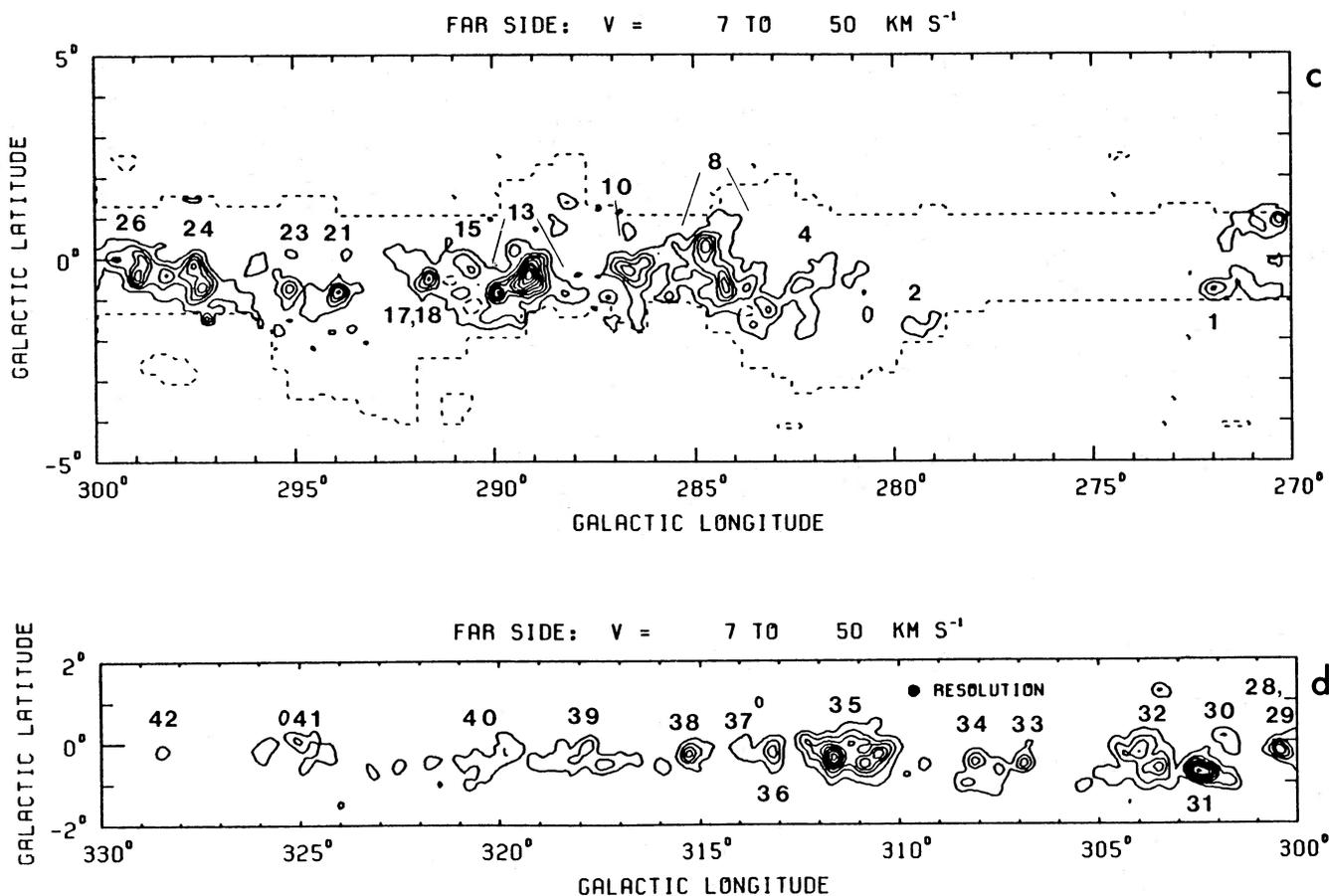FAR SIDE: V = 7 TO 50 KM S⁻¹

FAR SIDE: V = 7 TO 50 KM S⁻¹

FIG. 2—Continued

$b = -1°5$ in the near side of the arm (Fig. 2a) are blended into a single peak at $(l, v) \approx (283°, -15 \text{ km s}^{-1})$ in the l, v map. A comparison of Figure 2a and 2b indicates that the cloud at $b = -1°5$ is continuous with the tangent region emission, while the feature at $b = +1°$ shows no continuation into the tangent region map; these two clouds were therefore considered distinct.

The association of giant molecular clouds with H II regions, OB associations, and other Population I objects provided an important tool for checking our cloud list. Clouds observed in the near side and the tangent region of the Carina arm are particularly susceptible to velocity blending, i.e., the creation of kinematic artifacts due to the overlap in velocity of unrelated small clouds along the line of sight. However, small molecular clouds are not typically the sites of massive star-forming regions, so tying the large objects we identified to sites of active star formation helped rule out the possibility that they are merely kinematic artifacts. The physical association of the giant molecular clouds on our list with star-forming regions in the Carina arm was inferred from angular proximity and similarity in velocity. Evidence of interaction between the molecular cloud and an adjacent H II region occasionally supplied an additional argument for association. In some cases, e.g., the η Carinae molecular cloud (discussed in § IIIc below), an apparent grouping of CO peaks in the l, v and spatial maps could be identified as a single complex on the basis of association with various optical objects known to be at the same distance.

The final catalog of molecular clouds in the Carina arm with masses generally greater than $10^5 M_\odot$ is given in Table 2; the clouds are identified in the spatial maps (Fig. 2) by their running numbers in the table (first column). Specific criteria used to distinguish each cloud, including identification of associated Population I objects, are given in the Appendix.

a) Distances

Distances to the molecular objects we have identified were determined for the most part kinematically and, when possible, from associated optical objects of known distance, with optical distances preferred. The four clouds identified in the near side all appear along the high-velocity ridge in the l, v diagram. Two of these were assigned optical distances; the other two were placed kinematically on the subcentral locus (i.e., the locus of points inside the solar circle [which maps into the high velocity ridge] where the line of sight is tangent to circular galactocentric orbits).

In the l, v map, the tangent region of the arm, which lies at a distance of 3–5 kpc, is indistinguishable kinematically from local emission. About half the clouds identified here could be given optical distances; resolution of the kinematic distance ambiguity for the others was based on (1) association with a radio H II region whose foreground H I absorption permits distance discrimination or (2) the empirical relation derived by Dame et al. (1986) between the radius (inferred from distance) and the observed velocity width of molecular clouds (see § IIIb below for the definition of cloud radius and velocity width).

For clouds in the far side of the arm beyond the solar circle,

TABLE 2

MOLECULAR CLOUDS IN THE CARINA ARM

No.[a]	l	b	v (km s^{-1})	Δv (km s^{-1})	r^b (kpc)	R_{eff} (pc)	M_{CO} ($10^5 M_\odot$)	M_{vir}	Associated Objects[c]
1[d]	270°.9	−0°.5	52	7	6.8	57	2.2	5.1	...
2	279.9	−1.6	35	5	7.1	37	1.0	2.1	...
3	281.4	−1.1	−5	13	3.2	101	22.5	37.5	G282.2−2.0, R45, R47, (R46)
4	282.0	−0.8	17	5	6.1	88	2.7	4.6	G282.0−1.2
5	282.9	1.3	−19	6	2.2	26	0.7	2.2	...
6	282.9	−0.7	−5	9	3.2	31	2.8	5.6	(R46)
7	283.8	0.0	−5	10	4.0	65	6.3	13.1	R48, R49, Wd 2
8	284.5	−0.2	12	8	6.6	123	20.3	14.9	(G282.20−1.0, H8)
9	285.3	0.0	0	10	5.3	88	4.5	17.4	(H18)
10	286.4	−0.3	14	8	7.5	84	8.3	9.9	...
11	287.5	−0.5	−19	10	2.7	66	6.7	13.6	η Car, N3324, N3293, IC 2581
12	288.6	1.5	−22	7	3.2	56	3.5	5.8	...
13	289.3	−0.6	22	15	7.9	132	31.2	64.9	R54a, G289.1−0.4, (MSH 11−6*1*A)
14	290.2	−0.2	−1	5	6.8	55	2.7	3.2	...
15	290.6	−0.2	15	10	8.7	80	4.3	15.1	(MSH 11−6*2*)
16	291.4	−0.2	−7	4	...	...	...	...	*Local dust cloud*
17	291.6	−0.4	15	10	7.2	73	4.1	14.1	N3603
18	291.6	−0.5	29	6	10.3	105	12.5	6.7	H58
19	292.6	−0.3	4	4	8.1	31	12.0	9.1	...
20	293.3	−1.4	−25	8	2.4	77	7.1	9.2	R60, R61, R62, N3576
21	294.0	−0.9	32	8	11.3	102	12.2	13.1	(SNR: G293.8+0.6)
22	294.4	−0.7	−3	10	8.0	109	12.2	22.0	...
23	295.1	−0.8	26	11	11.0	64	4.5	16.3	(G295.2−0.6)
24	297.4	−0.5	22	18	11.2	154	32.1	102	(SNR: G296.8−0.2)
25	298.6	0.1	−35	10	4.7	139	26.5	26.3	...
26	298.8	−0.2	25	16	12.0	157	30.8	83.5	G298.2−0.3, G298.4−0.4, (SNRs: G298.5−0.3, 298.6+0.0, 299.0+0.2)
27	299.4	−0.1	−6	9	9.4	66	4.6	12.0	...
28	300.3	−0.2	31	9	12.9	61	7.0	10.4	G300.5−0.2
29	300.6	−0.2	10	7	11.1	61	4.2	6.4	G300.5−0.2 (H$_2$CO absorption)
30	301.8	0.0	24	7	12.7	44	4.2	4.5	...
31	302.3	−0.7	32	11	13.6	97	29.4	24.6	G302.5−0.7
32	303.9	−0.4	29	13	13.7	144	46.2	51.1	G303.1−0.9, G303.5−0.7
33	306.9	−0.5	25	7	14.2	50	5.6	5.2	...
34	308.0	−0.7	32	11	15.1	113	21.0	28.7	...
35	311.3	−0.3	27	17	15.5	210	109.2	127	G310.8−0.4, G311.1−0.3, G311.6−0.6
36	313.2	−0.3	42	10	17.6	100	18.2	21	...
37	314.0	−0.1	28	7	16.4	59	4.2	6.1	...
38	315.3	−0.3	14	10	15.4	72	11.2	15.1	G315.3−0.3
39	318.0	−0.3	30	15	17.6	148	2.8	69.9	G318.1−0.5
40	320.5	−0.5	26	17	17.8	155	12.6	94.1	...
41	325.3	−0.1	28	12	19.3	115	19.6	34.8	G325.0−0.6
42	328.5	−0.1	30	6	20.4	55	5.6	4.2	...
43	335.5	−0.5	27	5	22.0	<24	>0.6	1.3	...

[a] Clouds 1–27 are from the present survey; clouds 28–43 are from the survey of Bronfman (1986).

[b] All distances are heliocentric. Distances for clouds 3, 7, 11, 13, 17, and 20 are optical; cloud 16 is associated with local dust cloud of unknown distance; all other distances are kinematic. Kinematic distance ambiguities were resolved by: the radius–line-width relation (Dame *et al.* 1986) for clouds 6, 14, 19, 22, 27; foreground H I absorption for cloud 9. Clouds 5, 12, 25 are at the tangent point (no ambiguity); all others lie beyond the solar circle (no ambiguity).

[c] MSH sources are SNRs; all others are H II regions unless indicated otherwise. Designations: R, RCW; H, Hoffleit; N, NGC; G, Galactic coordinates. Parentheses indicate uncertain associations. See the Appendix for details.

[d] This cloud is probably not in the Carina arm; see the Appendix.

kinematic distances are single valued; only two clouds there could be assigned optical distances. A few clouds near zero velocity at longitudes higher than that of the tangent region were assigned distances according to the radius–line-width relation, the proximity to the $b = 0°$ plane, or by the probable association with local dust clouds.

b) Masses

Cloud masses were determined from CO luminosities on the empirically based assumption that the integrated CO line intensity, $W(CO) \equiv \int T_R \, dv$, is proportional to $N(H_2)$, the column density of H_2 along the line of sight (e.g., Lebrun *et al.* 1983; Bloemen *et al.* 1986; Sanders, Solomon, and Scoville 1984) and on the additional assumption that the hydrogen in

molecular clouds is entirely molecular. As in Paper I, we adopt the ratio derived by Bloemen *et al.*,

$$N(H_2)/W(CO) = 2.8 \times 10^{20} \text{ cm}^{-2} \text{ (K km s}^{-1})^{-1}, \quad (1)$$

and a mean molecular weight per H_2 molecule of $2.76 m_H$ (Allen 1973). The total mass of a molecular cloud (including helium) is then given by

$$M_{CO} = 1.9 \times 10^3 I_{CO} r^2 \; M_\odot, \quad (2)$$

where r is the heliocentric distance to the cloud in kpc and I_{CO} the total integrated emission over the face of the cloud in units of K km s^{-1} deg^2. In practice, I_{CO} has been determined by integrating the emission over the full velocity extent of the

cloud, as exhibited in the l, v diagram, and over the face of the cloud, defined by its lowest ($\sim 3 \sigma$) contour in the spatial maps.

For comparison, a virial mass, $M_{\rm vir}$, for each cloud was computed by assuming the cloud to be in virial equilibrium, i.e., supported against gravity purely by internal motion. For a spherical cloud of uniform density, radius R, and three-dimensional (isotropic) velocity dispersion σ, the virial theorem can be written as $M_{\rm vir}\sigma^2 - 3/5G(M_{\rm vir})^2/R = 0$, if magnetic or other nongravitational forces of pressure are negligible. For the molecular cloud radius, we take $R = R_{\rm eff} \equiv (A/\pi)^{1/2}$, where A is the projected area of the cloud determined from the spatial maps. We define the observed velocity width of the cloud, Δv, as the FWHM of a Gaussian fit to the cloud's "composite" spectrum, i.e., the sum of all spectra across the cloud's projected surface. On the assumption that Δv measures the cloud's internal motion, σ and Δv are then related by $\sigma = [3/(2 \ln 2)]^{1/2}\Delta v/2$. Solving for $M_{\rm vir}$, and substituting more convenient units, gives

$$M_{\rm vir} = 210R_{\rm eff}\Delta v^2 \, M_\odot \, , \qquad (3)$$

with $R_{\rm eff}$ in pc and Δv in km s^{-1}. If the cloud is not gravitationally bound and there is a contribution to the observed velocity width from disruption, e.g., by star formation, the expression for $M_{\rm vir}$ will overestimate the actual mass. Considering these possible qualifications, the virial mass as defined here will be taken to be an upper limit to the true mass of the cloud, but one probably within a factor of ~ 2 of the true mass.

c) The η Carinae Molecular Cloud

The general procedure used to identify and define molecular clouds in the survey is illustrated by considering the large complex of gas associated with the η Carinae nebula (NGC 3372), one of the brightest giant H II regions in the Galaxy and one of the most interesting and best-studied objects in the Carina arm. In the map of the near side of the arm (Fig. 2a), a string of five CO clouds is seen lying approximately on a line from $(l, b) = (285°, 0°5)$ to $(288°, -1°)$. The same group can also be seen at about -20 km s^{-1} in the l, v map (Fig. 1) between 285° and 288°. (The cloud at $[l, b] = [288°, 1°5]$ in Fig. 2a blends with the rest of the group in the l, v map.) The near side of the arm between these longitudes is the location of the Carina OB1 association at ~ 2.7 kpc, which consists of several star clusters and H II regions, including the η Carinae nebula.

Figure 3 shows a section of the near side of the arm (full-resolution, unsmoothed CO data) superposed on a mosaic of the ESO J plates of the same region. The η Carinae nebula is the bright H II region between $l = 287°$ and 288°; the young clusters Tr 14, Tr 16, and Cr 228, which altogether contain at least 16 main-sequence O stars (Walborn 1971, 1973), are thought to supply the ionizing radiation for the nebula. All three clusters are at ~ 2.7 kpc (Turner et al. 1980; Feinstein, Marraco, and Muzzio 1973; Walborn 1973) and are less than 3×10^6 yr old, perhaps even less than 10^6 yr old (Feinstein, Marraco, and Forte 1976; Turner et al. 1980). Like many other H II regions associated with giant molecular clouds, such as the Orion Nebula (e.g., Kutner et al. 1977), W3 (Lada et al. 1978), and the Rosette nebula (Blitz and Thaddeus 1980), the Carina nebula is apparently situated at the edge of a molecular cloud. Additional evidence of a close physical association is the near agreement of the mean H II velocity of -20 km s^{-1} from radio recombination line measurements (e.g., Wilson et al. 1970) with the mean CO velocity of -19 km s^{-1}. There is also evidence

for direct interaction between the H II region and the molecular cloud: the velocity structure of the molecular gas in the vicinity of the Carina nebula indicates that a portion of the cloud associated with the prominent dust lane seen in front of the bright ionized gas is being expelled from the main body of the molecular cloud at a speed of ~ 7 km s^{-1} (Grabelsky, Cohen and Thaddeus 1986). A detailed discussion of this and other issues, and of star formation in the Car OB1 association generally, is deferred to a later paper.

The cluster NGC 3324 at $(l, b) = (286°2, -0°2)$ is seen (Fig. 3) between two CO peaks and along a CO ridge in Figure 3; it is only $\sim 2.2 \times 10^6$ yr old according to Claria (1977) and contains at least one O6–7 star (Goy 1973). The associated Hα region G31, apparently ionized by the bright stars in the cluster (Gum 1955), has a velocity of -19.4 km s^{-1} (Georgelin, Lortet, and Testor 1986). The CO emission in this direction peaks at about -20 km s^{-1}, providing further evidence for association between NGC 3324 and the nearby molecular cloud. Estimates of the distances to NGC 3324 and G 31 range from 1.9 to 3.28 kpc (Humphreys 1976; Hoffleit 1953; Georgelin 1975; Turner et al. 1980; Claria 1977; Moffat and Vogt 1975), with an average of 2.7 kpc, the distance to the Carina nebula and therefore consistent with membership in Car OB1. It may therefore be concluded that the molecular clouds associated with the Carina nebula and NGC 3324 are components of a single, giant-cloud complex at 2.7 kpc.

Another nearby cluster, NGC 3293 (285°9, 0°1), and its accompanying Hα region G30 are seen toward a steep ridge of CO emission. The cluster has an age of $\sim (5–10) \times 10^6$ yr according to Turner et al. (1980) and Stothers (1972), so it is apparently somewhat older than NGC 3324. The Hα velocity of G30 is -18.5 km s^{-1} (Georgelin, Lortet, and Testor 1986), in good agreement with the velocity of -20 km s^{-1} for the molecular cloud. Again, the distance is ~ 2.7 kpc (e.g., Humphreys 1972; Turner et al. 1980). We conclude that NGC 3293, another member of Car OB1, is probably associated with the same cloud complex as the Carina nebula and NGC 3324.

This cloud complex may also include the molecular cloud at (285°2, 0°4), on the assumption of an association of the latter with the cluster IC 2581 (284°7, 0°1), also at ~ 2.7 kpc (Turner 1978). Stothers (1972) estimates an age of $\sim 10^7$ yr for IC 2581, which suggests that it is part of the oldest generation of star formation in Car OB1. The radial velocity of IC 2581 is -13.7 km s^{-1} (Humphreys 1972), while the strongest CO emission of the adjacent cloud lies between -23 and -21 km s^{-1} (Grabelsky 1985); the uncertainty in the velocity of the cluster, however, is probably of the order of this difference. An association is still possible, and this cloud, too, may be part of the η Carinae molecular complex.

It is reasonable to conclude, therefore, that nearly all CO emission in the near side of the arm between $l = 284°7$ and 289° originates in a single, giant molecular cloud complex. At a distance of 2.7 kpc, the projected length of this complex is ~ 150 pc, typical of the largest complexes in the first and second quadrants. The clusters discussed above have previously been considered to define the Car OB1 association (e.g., Lyngå 1970). Turner et al. (1980) emphasized that the sequential orientation of the clusters along the Galactic plane and an apparent age gradient from the young clusters in the Carina nebula to the older IC 2581 are evidence for a common origin. The large molecular cloud complex we postulate is therefore plausibly the parent material of the entire Carina OB1 association.
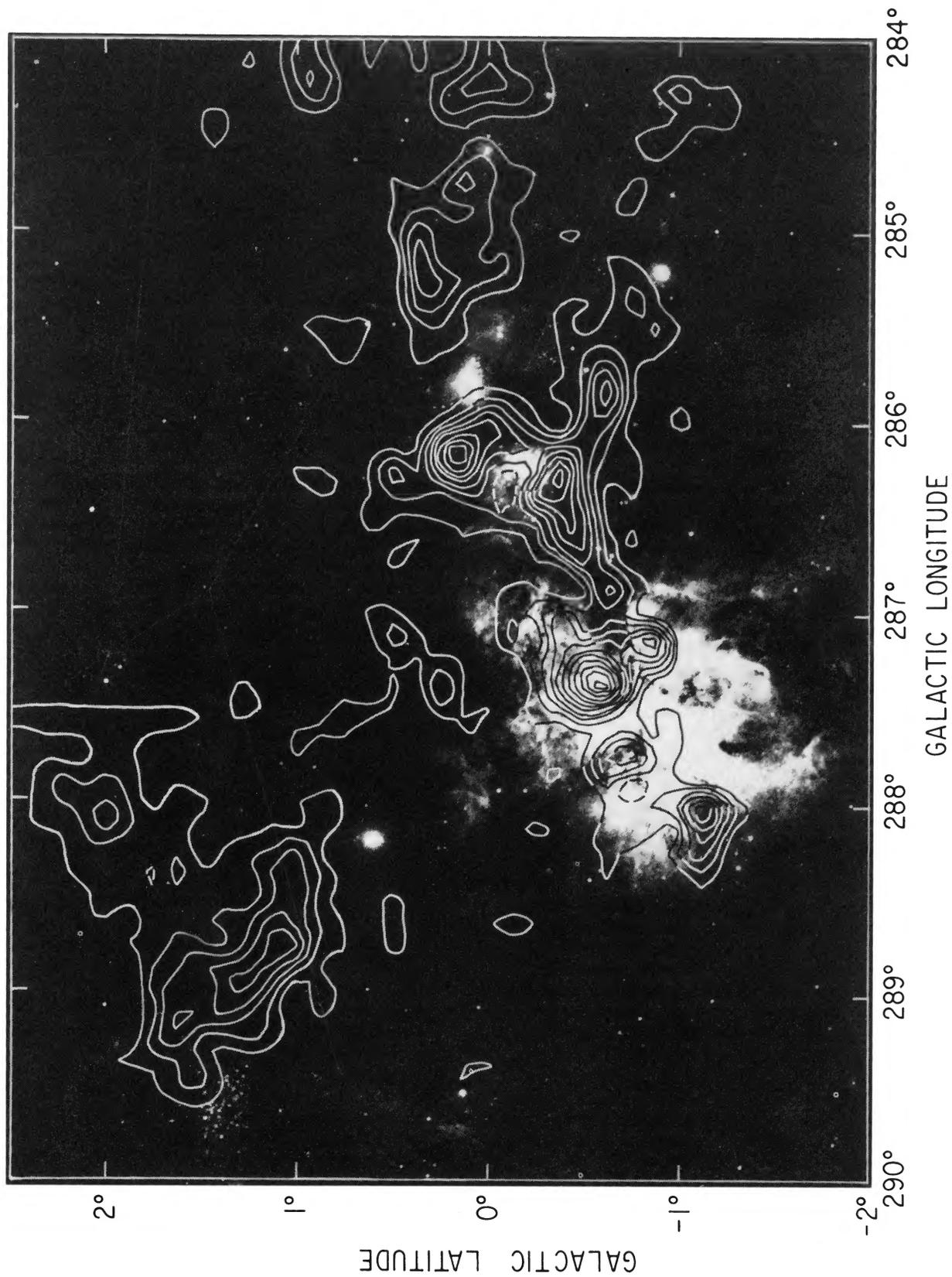
Fig. 3.—Optical mosaic of the η Carinae nebula and its surroundings from ESO J plates of the region. The CO contours overlaid on the mosaic are full-resolution data inside the dotted line and low-resolution data beyond; the emission is integrated from -50 to -9 km s^{-1}, and the contour interval is 5 K km s^{-1}.

Making use of equation (2), we find that the CO mass of the cloud complex is substantial, $6.7 \times 10^5 \, M_\odot$, but still somewhat smaller than that of the largest molecular complexes in the Galaxy. With a full velocity width, Δv, of 9.9 km s^{-1} and an effective radius, $R_{\rm eff}$, of 66 pc, the virial mass of the cloud complex from equation (3) is $1.4 \times 10^6 \, M_\odot$. The discrepancy between the CO and virial masses is in the sense expected if the virial mass is an upper limit, and suggests that this complex may be an example of one in which disruption due to vigorous star formation contributes to the observed velocity width.

d) Completeness of the Cloud Catalog

In Paper I the projected surface density of H_2 in the Galactic plane averaged between longitudes 280° and 335° was derived as a function of galactocentric radius between $R = 10.5$ and 13.0 kpc, yielding a total mass of molecular hydrogen of $(1.0 \pm 0.1) \times 10^8 \, M_\odot$ for this section of the outer Galaxy. The completeness of our catalog is evaluated by comparing this sum to the total mass contained in those molecular clouds in the catalog at $l > 280°$ and beyond the solar circle ($v > 0$). For these clouds we find a total mass of $4.8 \times 10^7 \, M_\odot$, a factor of ~2 smaller than that derived in Paper I. The difference can be reconciled largely by taking into account (1) molecular clouds too small to be included in the catalog and (2) a few molecular clouds interior to the Carina arm that contribute to the surface density derived in Paper I but that are not included in our catalog of Carina arm clouds. Clouds in category (2) may lie in a distant portion of the Centaurus arm (Bronfman 1986) and contain in total as much as $10^7 \, M_\odot$ (Bronfman, private communication). From the mass spectrum for molecular clouds obtained by Dame et al. (1986), ~$1.4 \times 10^7 \, M_\odot$ of molecular hydrogen is estimated to reside in clouds below the mass threshold for inclusion in our catalog here. With corrections (1) and (2), the total cloud mass found from cloud counting is the same to within 15%–25% as that derived from the axisymmetric averaging of CO emission in Paper I.

This agreement is entirely satisfactory, and it indicates that for giant molecular clouds of $10^5 \, M_\odot$ or greater within the section of the outer Galaxy considered here and in Paper I, our catalog is largely complete. In § IV all of these clouds are shown to lie in the Carina arm. If the Centaurus-arm clouds are neglected, and the total mass contained in clouds below the threshold is assumed to be distributed equally between the Carina arm and its surrounding interarm regions, then the deduced arm-interarm contrast by mass is nearly 8:1. This result is consistent with the more directly obtained value of 13:1 derived in Paper I from the step in intensity of the integrated CO emission, $\iint T_R \, dv \, db$, seen at the longitude of the tangent direction, and demonstrates again the high degree of concentration of molecular clouds to Galactic spiral arms.

IV. DISCUSSION

The question of how the Carina arm fits into the overall spiral structure of the Galaxy was apparently first raised by Bok (1937), who proposed that a single spiral arm could be traced from Carina through Cygnus. Early hopes that 21 cm studies would settle the matter have been frustrated by the ubiquity of H I, the kinematic distance ambiguity within the solar circle, and the difficulties introduced by possible non-circular motions. Further, for regions more than a few kiloparsecs from the Sun the inability to check structure derived kinematically against structure derived from optical tracers is aggravated by the difficulty of observationally linking regions

of active star formation to the H I. The H I counterpart of the Carina arm has been recognized since the earliest 21 cm surveys, yet the question of how the Carina arm fits in with the general spiral pattern of the Galaxy has remained open ever since Bok's original suggestion (which preceded the 21 cm observations by some 20 yr) of a Carina-Cygnus arm.

Weaver (1970) proposed a model based on 21 cm observations in which the Carina and Sagittarius arms were seen as different segments of a single major spiral arm with a pitch angle of ~12°5. At about the same time, Kerr (1970) proposed a model similar to Bok's, in which the Carina and Cygnus arms form a low-pitch spiral; in his model, also based on 21 cm data, there must be a localized region of low density where the arm passes through the solar neighborhood (Simonson 1970). As evidence against a Carina-Sagittarius arm, Kerr and Kerr (1970) pointed to a gap between $l = 292°$ and 305° in the 11 cm continuum and H109α fluxes and argued that such an arm would be expected to pass just *inside* the solar circle in this longitude range. They maintained instead that the only H II regions seen in this gap were distant and could not represent a connecting segment between Carina and Sagittarius. More recently, Henderson, Jackson, and Kerr (1982) presented maps of H I surface density projected onto the Galactic plane in which the Carina arm appears to remain *outside* the solar circle even at longitudes less than 280°.

From the distribution of luminous stars, associations, clusters, and H II regions, Humphreys (1976) traced the Carina arm into the first quadrant where, like Weaver, she suggested that it joined the Sagittarius arm. Georgelin and Georgelin (1976), using optical and radio H II regions as tracers, also proposed a Carina-Sagittarius arm. However, toward the Galactic center where the arm passes just inward of the Sun, they found that the distribution of nearby H II regions does not trace the arm very clearly—but it does largely fill in the gap in nearby H II regions which worried Kerr and Kerr (1970). Further, an apparent absence of H II regions along ~6 kpc in the Sagittarius segment between $l \approx 30°$ and 45° is difficult to reconcile with the claim of large-scale continuity.

The distribution of the largest molecular clouds—those more massive than ~$10^5 \, M_\odot$—in projection on the Galactic plane suggests rather forcefully that the Carina and Sagittarius arms are connected. Figure 4a shows all the Carina clouds generally more massive than $10^5 \, M_\odot$, as well as similarly massive clouds identified in earlier CO surveys made with the New York Telescope. In the first and second quadrants, the Perseus and Sagittarius arms are apparent. In the fourth quadrant, the dominant feature is the Carina arm, traced over a path length of 23 kpc by 37 clouds with an average mass of $1.4 \times 10^6 \, M_\odot$ and an average intercloud spacing of 700 pc along the arm. Details given in the Appendix indicate that although not every Carina-arm cloud appears to have associated Population I objects, the main radio and optical tracers of the classic Carina arm between $l = 280°$ and 300° are invariably associated with molecular clouds. From the figure it is clear that, except for a short stretch along the near side of the arm between $l = 300°$ and 12°, the Carina and Sagittarius features appear to form a continuous spiral arm.

In the shaded, wedge-shaped area in Figure 4a from $l = 300°$ to 12° (a region which has been surveyed in CO with the Chile Telescope [Bronfman 1986], but which remains only partially analyzed), the path length along the Carina arm is ~1 kpc, only slightly larger than the average spacing between the largest clouds. The dip in the radio continuum and H109α
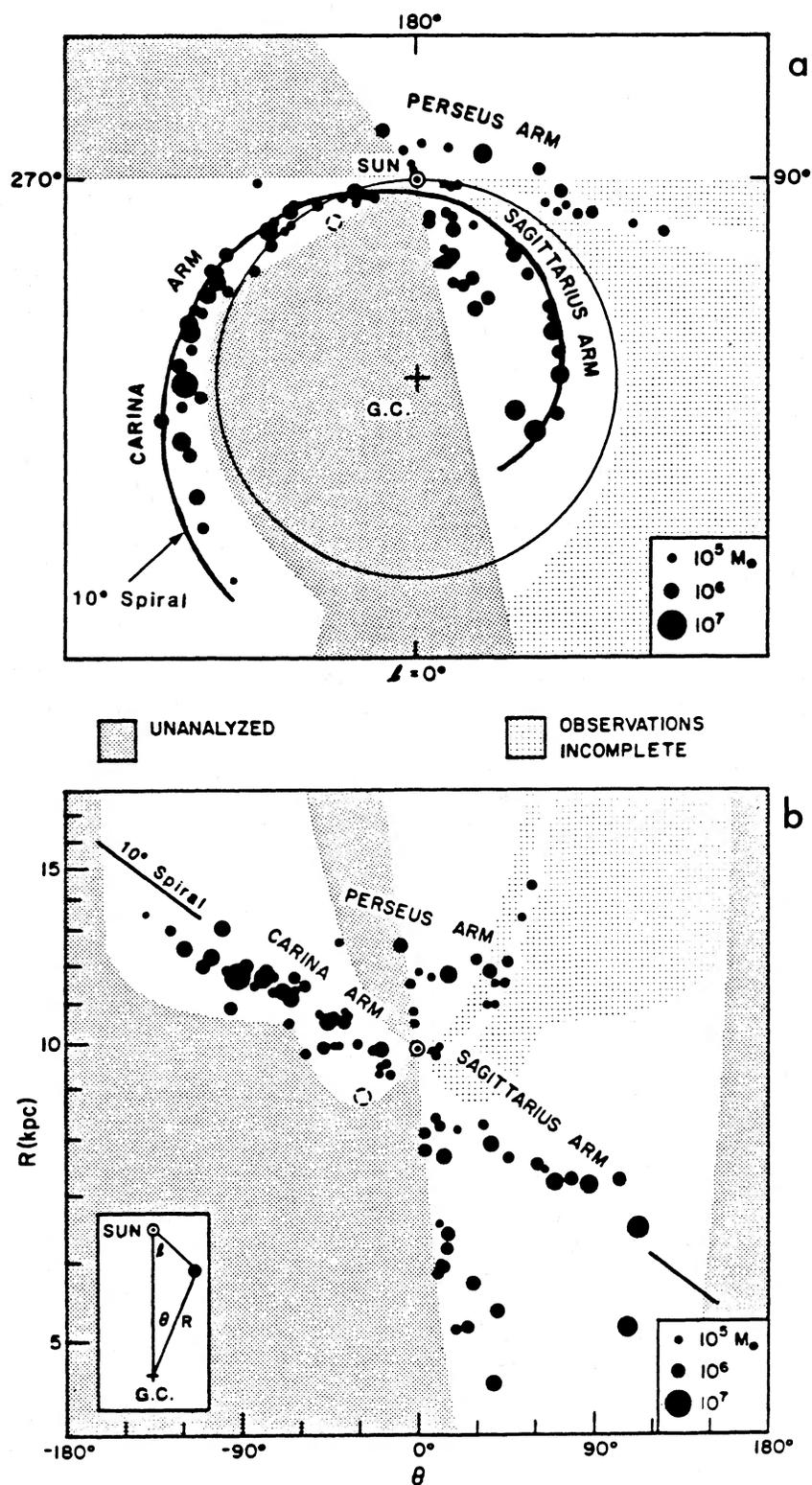
FIG. 4.—(a) Face-on view of the Galaxy with the locations of the largest molecular clouds. The cloud shown with a dashed circle has a very inaccurate distance and may actually lie in the Carina arm (see Appendix, cloud no. 25). The dark line is a 10° logarithmic spiral that crosses the solar circle at $l = 281°$. In the shaded region in the fourth quadrant labeled "unanalyzed," the inventory of giant molecular clouds is not yet complete, although the average radial distribution of molecular clouds has been determined here (Bronfman et al. 1987). (b) Same as in (a) but replotted in rectangular semilog coordinates. The line shows the same logarithmic spiral as in (a).

190

fluxes between $l = 292°$ and $305°$ which was noted by Kerr and Kerr falls within this wedge, but it has no counterpart in reduced CO emission; rather, the l, v and spatial maps show the near side of the arm continuing well into the inner-Galaxy emission, where it becomes difficult to trace. The gap in Figure 4a between the Carina and Sagittarius arms is bridged optically by young clusters (Vogt and Moffat 1975), giant stars (Humphreys 1976), and weak H II regions (Georgelin and Georgelin 1976), as well as a tentatively identified molecular cloud between $l = 345°$ and $346°$ (Bronfman 1986). A large gap between the clouds in the near side of the Carina arm and those in the direction of Cygnus ($l \approx 80°$), also apparent in the figure, is not similarly bridged by Population I objects. The near side of the Carina arm would have to spiral outward from $l = 300°$ to $\sim 80°$ to meet Cygnus, making any connection of the Carina and Cygnus arms quite unlikely.

The mass densities per unit distance along the Carina and Sagittarius arms are nearly equal, consistent with the idea that they are part of a larger arm. The total cloud mass in the Carina arm, $58 \times 10^6 \, M_\odot$, extends over 23 kpc, for a linear mass density of $2.5 \times 10^6 \, M_\odot \, pc^{-1}$; in the Sagittarius arm, a total mass of $39 \times 10^6 \, M_\odot$ extends over 16 kpc, again for $2.5 \times 10^6 \, M_\odot \, pc^{-1}$. In Perseus, by contrast, $9.8 \times 10^6 \, M_\odot$ is distributed over a distance of 8 kpc, for a linear density of only $1.3 \times 10^6 \, M_\odot \, pc^{-1}$—lower by a factor of 2.

In a plot of galactocentric angle versus the logarithm of galactocentric radius (Fig. 4b), where a logarithmic spiral appears as a straight line, the continuity of the Carina and Sagittarius arms is even clearer. All the Carina and Sagittarius clouds fall close to a $10°$ spiral (the best-fit pitch angle is $9°.75$), with a tangent at $l = 281°$. Drawn in the Galactic plane (Fig. 4a), this spiral emphasizes the continuous Carina-Sagittarius spiral arm traced by the largest molecular clouds. Adopting the new IAU values of R_0 and V_0 (with a flat rotation curve beyond R_0) leaves the picture essentially unaltered, i.e., the pitch angle and phase of the spiral do not change.

V. CONCLUSION

The main conclusion of this paper is that the Carina and the Sagittarius arms form a single spiral arm nearly 40 kpc in length extending at least two-thirds of the way around the Galaxy. Although the suggestion of a Carina-Sagittarius arm is not new, the combined distribution of the largest molecular clouds in the northern and southern Galactic plane offers the firmest evidence to date for this picture of Galactic spiral structure. Liszt and Burton (1981) have cautioned that streaming motions associated with a spiral velocity field can give rise to loops and mimic large objects in the CO l, v diagram, much as they can in the H I. But nearly all of the molecular complexes we have identified in the Carina-Sagittarius arm are associated with known star-forming regions; in the Carina arm, in particular, many of these young stars and H II regions are observed optically to 10 kpc and beyond. The possibility is therefore remote that the large objects we have identified in CO are

kinematic artifacts whose associations in space and velocity with sites of active star formation are merely coincidental. On the contrary, the demonstration of such a large-scale spiral arm from the combined north-south distribution lends strong support to the claim that giant molecular clouds are good tracers of Galactic spiral structure. The demonstration in Paper I that the arm-interarm contrast toward the Carina arm tangent is 13:1, independent of velocity and therefore of streaming motions, is crucial additional evidence for this conclusion.

Our inventory of clouds more massive than $10^5 \, M_\odot$ in the region of the Galaxy through which the Carina arm passes is probably fairly complete. Essentially all of these clouds lie in the Carina arm, and the mass spectrum determined by Dame et al. (1986) predicts that they account for $\sim 85\%$ of the arm's total molecular cloud mass. The degree to which the detailed structure of each cloud can be studied obviously depends on distance, and the most distant clouds in our sample are poorly resolved. The high total luminosities of the largest molecular clouds, however, make them fairly conspicuous, and the Galactic distribution of giant molecular clouds can generally be studied without fully resolving their internal structure. Our goal of delineating the largest molecular objects in the Carina arm has apparently been attained.

The close association of star-forming regions with molecular clouds in the Carina arm discussed here and the fairly tight correlation between the CO and the H I demonstrated in Paper I provide an observational connection between star formation and H I within the Galaxy on a very large scale. In the distant stretch of the Carina arm, beyond the solar circle, the giant molecular clouds appear to be located at the cores of much larger H I concentrations (Paper I). This may have interesting implications for mechanisms of molecular cloud formation (Elmegreen 1987). Further study of the relationship between giant molecular clouds and large H I clouds in the Carina arm may bear on questions of molecular cloud formation, star formation, and spiral structure in the Galaxy.

With the completion of the well-sampled Columbia CO surveys of the northern and southern Milky Way, the study of Galactic spiral structure from CO has evolved from tracing loops in the l, v diagram to identifying distinct giant molecular cloud complexes that trace spiral structure on a Galactic scale, just as O and B stars first traced it locally (Morgan, Sharpless, and Osterbrock 1952; Morgan, Whitford, and Code 1953). The reliability of CO as a Galactic spiral tracer is nowhere better demonstrated than in the Carina arm.

APPENDIX

NOTES ON INDIVIDUAL CLOUDS

Table 2 is a catalog of the molecular clouds identified between $l = 270°$ and $300°$ in the present survey, as well as the clouds in the far side of the Carina arm beyond $l = 300°$ identified in the supplementary CO survey made by Bronfman (1986) with the same telescope. The catalog is ordered by increasing longitude; the number in the first column identifies each cloud in both the spatial

maps (Fig. 2) and the notes in this Appendix. The other columns list, respectively: Galactic coordinates, radial velocity (with respect to the local standard of rest), velocity width, heliocentric distance, effective radius, CO mass, virial mass, and associated objects, if any. The notes below summarize cloud identifications, distance determinations, and identification of associated objects. Occasional reference is made to l, v maps at single latitudes, which may be found in Grabelsky (1985).

All of the clouds at $l > 300°$ lie beyond the solar circle and have single-valued kinematic distances; no further explanation of distance determinations is given in the notes for these clouds. Most are distinct features in the survey and require little discussion regarding identification, but half were found to be associated with very distant H II regions recently cataloged by Caswell and Haynes (1987, hereafter CH). The recombination line velocities given by CH are averages of the H109α and H110α lines observed toward target radio-continuum sources.

1. $l = 270°.9, b = -0°.5, v = 52$ km s^{-1}.—The velocity of this cloud makes its kinematic distance single valued and indicates that it lies beyond the solar circle. No associated objects have been identified. Its longitude, $\sim 10°$ below that of the Carina tangent (at $l \approx 280°$), and its distance indicate that it does not lie in the Carina arm. This cloud may be related to the H I feature in the outer Galaxy noted in Paper I, Figures 11 and 13.

2. $l = 279°.9, b = -1°.6, v = 35$ km s^{-1}.—This very weak feature has no associated objects. Its kinematic distance is single-valued and places it beyond the solar circle.

3. $l = 281°.4, b = -1°.1, v = -5$ km s^{-1}.—We classified this object in the tangent region as a cloud complex, but owing to velocity crowding it may include quite unrelated objects. Spatial maps of this region (Fig. 2b; Paper I, Fig. 7b) and the l, v map (Fig. 1) show several peaks between $l = 280°$ and $283°$, and the overall nature of the emission appears highly confused. With the two exceptions noted below, no attempt was made to sort out the various components in this region.

This cloud complex appears to be associated with the H II region G282.2−2.0 at 3.2 kpc (Bigay *et al.* 1972). The Hα velocity of G282.2−2.0 is −12.2 km s^{-1} (Bigay *et al.*), slightly less than the CO peak in its direction.

Three other H II regions between $l = 280°$ and $283°$, RCW 45, RCW 46, and RCW 47, may also be associated with various components of this cloud. RCW 45 (282°.2, −0°.1) is observed near the CO peak at (282°.3, −0°.5); its Hα velocity is −9.8 km s^{-1} (Bigay *et al.* 1972). No optical distance is available. RCW 47 (283°.0, 2°.7) at 2.7 kpc (Georgelin 1975) is seen toward the weak emission at the low latitude edge of the cloud; its Hα velocity is −11.6 km s^{-1} (Bigay *et al.* 1972). RCW 46(282°.4, −1°.3) at 1.8 kpc (Georgelin 1975) is observed between two CO peaks at (281°.7, −1°.5) and (282°.75, −1°.25); its Hα velocity is −10.6 km s^{-1} (Georgelin 1975). The second of the CO peaks, a fairly distinct feature both in the integrated l, v map (Fig. 1) and in l, v maps at each latitude between −1°.5 and 0° (not shown here), was cataloged as a separate cloud in the list, no. 6. It is not clear whether RCW 46 is associated with cloud no. 3 or no. 6.

Another object (aside from cloud no. 6) tentatively identified in the complicated CO emission near the tangent point of the Carina arm is cloud no. 5 at (282°.9, 1°.3). In the spatial maps almost no emission from this object extends across the boundary between the near side and the tangent region (Figs. 2a, b; Paper I, Figs. 7a, b), implying that it is a distinct cloud.

After excluding the emission from no. 5 and no. 6, the remaining emission for no. 3 yields a CO mass of $2.3 \times 10^6 M_\odot$. Although its apparent CO luminosity may be slightly elevated by "local" emission from quite near the Sun, the derived CO mass for this cloud complex is not atypical of other large complexes in the Galaxy.

4. $l = 282°.0, b = -0°.8, v = 17$ km s^{-1}.—This cloud has a single-valued kinematic distance and thus lies beyond the solar circle. The H II region G282.0−1.2, with an H109α recombination line velocity of 22.4 km s^{-1} (Wilson *et al.* 1970) and an Hα velocity of 21.6 km s^{-1} Bigay *et al.* (1972), is observed in the same direction, but no optical distance determination is available.

5. $l = 282°.9, b = 1°.3, v = -19$ km s^{-1}.—No known H II regions, continuum sources, OH or H$_2$CO emission or absorption features, or apparent optical obscuration are seen toward this cloud. Its velocity places it near the subcentral point.

6. $l = 282°.9, b = -0°.7, v = -5$ km s^{-1}.—This cloud is fairly distinct in the l, v map at $(l, v) = (282°.9, -5$ km s$^{-1})$ and was therefore considered to be separate from cloud no. 3. Association with RCW 46 is possible, but not compelling. The cloud was assigned the far kinematic distance on the basis of the radius-line-width relation (Dame *et al.* 1986).

7. $l = 283°.8, b = 0°.0, v = -5$ km s^{-1}.—This cloud is probably associated with RCW 48 and RCW 49, placing it at 3–5 kpc. These two nebulae may actually be part of a single H II region complex (Bigay *et al.* 1972). RCW 48(283°.5, −1°.0) appears near the edge of the molecular cloud and has a mean Hα velocity of −8.2 km s^{-1} (Bigay *et al.*). Its cresent shape in both the optical and in the radio continuum (Shaver and Goss 1970) suggests that the concave side of the crescent is not due to obscuration but instead marks the boundary with the molecular cloud.

RCW 49 consists of an optically bright central portion coincident with a strong radio-continuum source at (284°.3, −0°.3) (Shaver and Goss 1970) surrounded by diffuse Hα emission extending $\sim 0°.5$ from the center. The center of RCW 49, midway between two CO peaks, has a mean Hα velocity of −7.8 km s^{-1} (Bigay *et al.* 1972) and an H109α recombination line velocity (measured only toward the continuum source) of −0.7 km s^{-1} (Wilson *et al.* 1970).

From the exciting stars, Georgelin (1975) estimates a distance of 3 kpc to both RCW 48 and RCW 49. From the distance to the apparently associated cluster Wd 2, Moffat and Vogt (1975) place RCW 49 at 5 kpc. Here a distance of 4 kpc is adopted, with an uncertainty of about ± 1 kpc.

8. $l = 284°.5, b = -0°.2, v = 12$ km s^{-1}.—The single-valued kinematic distance of this cloud places it beyond the solar circle. The radio-continuum source G282.0−1.0, near the one of the cloud's two CO peaks, has an H109α recombination line velocity of 4.5 km s^{-1} (Wilson *et al.* 1970). The weak Hα source H8, also coincident with the radio source, may be related to it and the molecular cloud, but the evidence is not compelling; no optical distance to H8 is available.

9. $l = 285°.3, b = 0°.0, v = 0$ km s^{-1}.—This cloud is evidently either very close to the Sun or near the solar circle at ~ 5.3 kpc. The far kinematic distance was chosen because H I absorption of a bright continuum source seen toward the cloud is due to nonlocal, intervening gas (Goss *et al.* 1972). The cloud's small size, moderately large line width, and low latitude also suggest the far distance. The small Hα source H18 is the apparent optical counterpart of the radio H II region.

10. $l = 286°4, b = -0°3, v = 14$ km s^{-1}.—This cloud has a single-valued kinematic distance and thus lies beyond the solar circle. It has no associated radio or optical objects.

11. $l = 287°5, b = -0°5, v = -19$ km s^{-1}.—This is the large cloud complex associated with the η Carinae nebula, NGC 3324, NGC 3293, and IC 2581. Its distance was taken to be 2.7 kpc, the distance to the associated objects. See the detailed discussion in § IIIc.

12. $l = 288°6, b = 1°5, v = -22$ km s^{-1}.—The kinematic distance to this object places it at the subcentral point. The filamentary Hα source RCW 54b appears at the edge of this cloud, but no velocity information is available so an association is moot.

13. $l = 289°3, b = -0°6, v = 22$ km s^{-1}.—This is one of the two clouds in the far side of the Carina arm for which an optical distance can be assigned. The H II region RCW 54a (289°7, $-1°3$), at 7.9 kpc (Georgelin and Georgelin 1970b), is seen near one of the two CO peaks of the cloud; its H109α recombination line velocity is 21.9 km s^{-1} (Wilson et al. 1970) and its Hα velocity is 20.7 km s^{-1} (Georgelin and Georgelin 1970b). Another H II region, G289.1−0.4, is seen directly toward the other CO peak with an H109α recombination line velocity of 27 km s^{-1} (Wilson et al. 1970); first identified as a nonthermal source by Milne et al. (1969), it was subsequently shown to be thermal by Shaver and Goss (1970). A third H II region toward the molecular cloud, G289.9−0.8, has an H109α velocity of 5 km s^{-1} (Dickel 1973) and is therefore presumably a foreground object.

Another object seen close to the smaller CO peak is the supernova remnant MSH 11−61A(290°1, $-0°8$), a bright radio-continuum source (Shaver and Goss 1970) with a faint optical shell (Kirshner and Winkler 1979; Elliot and Malin 1979). Its distance is estimated to be 3.2–5.8 kpc, although a substantially greater distance is possible (Kirshner and Winkler 1979; Elliot and Malin 1979).

14. $l = 290°2, b = -0°2, v = -1$ km s^{-1}.—The far kinematic distance was assigned to this cloud on the basis of its small angular size, its proximity to the Galactic plane, and the radius–line-width relation (Dame et al. 1986). Possible association with the optical H II region G37 (RCW 54c) observed toward the cloud's edge seems ruled out by the Hα velocity of about -22 km s^{-1} (Georgelin and Georgelin 1970b).

15. $l = 290°6, b = -0°2, v = 15$ km s^{-1}.—The composite spectrum of this feature shows two velocity components at ~ 9 and 18 km s^{-1}, although the only evidence for two components in the individual spectra of this object is slightly asymmetric line profiles at a few positions. Only one object is apparent in the l, v and spatial maps, so this feature was classified as a single cloud. Its kinematic distance, 8.7 kpc, is single valued and places the cloud beyond the solar circle. The supernova remnant MSH 11−62(291°0, $-0°1$), at an estimated distance of 9.9 kpc (Milne 1979), lies near the edge of the cloud; an association is therefore possible.

A weak, nonthermal continuum source, G290.4−0.9, offset slightly from the cloud's edge, is probably extragalactic (Shaver and Goss 1970).

16. $l = 291°4, b = -0°2, v = -7$ km s^{-1}.—This feature matches fairly well a dark dust cloud on the ESO J plate, so there can be little doubt that the CO emission is local. Sandqvist (1977) finds this dust cloud (no. 127 in his Table 1) among the darkest in a survey of 95 dark clouds. It has also been detected in formaldehyde absorption with a velocity of -6.5 km s^{-1} (Goss et al. 1980). The virtual absence of stars near the dust cloud's core implies that the object is extremely close. Although it clearly does not lie in the Carina arm, we include this cloud in our catalog as an example of low-velocity clouds found to be local.

17. $l = 291°6, b = -0°4, v = 15$ km s^{-1}.—This cloud is almost certainly associated with the giant H II region NGC 3603 which lies directly toward the CO peak and has an H109α recombination line velocity of 9.5 km s^{-1} (Wilson et al. 1970). Optical distance determinations to the H II region range from 7–8 kpc; we adopt van den Bergh's (1978) measurement of 7.2 kpc for the molecular cloud. Apparently the most massive optically visible H II region in the Galaxy (Goss and Radhakrishnan 1969), NGC 3603 has drawn considerable interest as a nearby analog of extragalactic giant H II regions, especially of the 30 Doradus H II region in the Large Magellanic Cloud (e.g., Walborn 1973; Balick, Boeshaar, and Gull 1980; Moffat 1983). From spectrophotometry of the exciting cluster, Moffat (1983) infers a stellar content roughly equivalent to 20 O5 stars, or $\sim 10^{51}$ Lyman-continuum photons per second, consistent with radio-continuum observations of the H II region (e.g., Goss and Shaver 1970). Balick, Boeshaar, and Gull (1980) find evidence for a wind-driven bubble in the dense core of the H II region and supersonic turbulence throughout. On the basis of the optical and infrared morphology of the nebula, Frogel, Persson, and Aaronson (1977) suggest that the massive stars in NGC 3603 have cleared away the dust and gas in their immediate vicinity.

In contrast to the spectacular H II, the mass of NGC 3603 giant molecular cloud, while substantial, is not especially large: $\sim 4 \times 10^5 \, M_\odot$. It is perhaps significant, however, that the virial mass of this cloud is more than 3 times its CO mass, possible evidence of stellar disruption. In addition to the already broad velocity width of the cloud, the composite spectrum shows a second velocity component redshifted by 14 km s^{-1}, suggestive of an even more massive and extremely disrupted molecular cloud complex. This interpretation finds some support in the virial mass of the combined system: at 7.2 kpc, the observed relative motion of the two components, together with the assumptions that they are separated by 100 pc and are gravitationally bound, implies a virial mass of $\sim 10^6 \, M_\odot$, in agreement with the combined CO masses. Because the two components appear quite distinct both in the l, v maps at single latitudes and in the composite spectrum, however, we tentatively cataloged the second (higher velocity) component separately as cloud no. 18. The entire region of these two molecular clouds merits further study.

18. $l = 291°6, b = -0°5, v = 29$ km s^{-1}.—The kinematic distance to this cloud is 10.3 kpc, although it may be part of a large complex at 7.2 kpc which includes cloud no. 17, as discussed immediately above. It appears to be associated with the H II region H58 (291°9, $-0°7$) which has an H109α recombination line velocity of 25.5 km s^{-1} (Wilson et al. 1970) and an Hα velocity of 22.3 km s^{-1} (Georgelin and Georgelin 1976). No optical distance is available for H58. At its kinematic distance, the cloud's CO mass exceeds its virial mass by a factor of ~ 2. If the distance is instead taken to be 7.2 kpc, the virial mass of the cloud then exceeds slightly its CO mass. A determination of the distance to the exciting stars in H58 would clearly be of great value in understanding the relationship of clouds 17 and 18 and their respective H II regions.

19. $l = 292°6, b = -0°3, v = 4$ km s^{-1}.—This weak feature has no counterpart as far as we can tell at other wavelengths. It was placed at the far kinematic distance on the basis of the radius–line-width relation.

20. $l = 293°3, b = -1°4, v = -25$ km s^{-1}.—This large cloud complex was placed at 2.4 kpc because of its apparent association with the bright H II region RWC 62 (also referred to as IC 2944, after the young cluster containing the ionizing stars), one of four associated H II regions. RCW 62 has an H109α velocity of -20.9 km s^{-1} (Wilson *et al.* 1970) and is seen at one end of the cloud, near $l = 295°$. Georgelin and Georgelin (1976) suggested that, with two other H II regions, RCW 60 and RCW 61, RCW 62 is part of a single H II region complex; the average Hα velocity of the three is -27.6 km s^{-1}, in good agreement with that of both the radio recombination line and CO. The distance to RCW 62 (IC 2944) is the best established of the three and is adopted here for the molecular cloud. The fourth H II region, NGC 3576, has an H109α velocity of -23 km s^{-1} (Wilson *et al.* 1970) and appears immediately next to a strong CO peak near $l = 291°5$. Various published optical distances to NGC 3576 place it between 2.5 and 3.3 kpc (Georgelin and Georgelin 1970b, 1976; Humphreys 1978), the uncertainty due in part to uncertain identification of the exciting stars (Y. M. Georgelin, private communication). It is plausible that NGC 3576 is at the same distance and associated with the same molecular cloud complex as RCW 60, RCW 61, and RCW 62. At 2.4 kpc, this giant molecular cloud has a projected length of ~ 160 pc ($R_{eff} = 77$ pc) and a mass of $7 \times 10^5 M_\odot$, both values typical of other large molecular objects in the Galaxy.

An alternative interpretation of this complex is that it consists of well-separated molecular clouds seen in projection, one associated with RCW 60, RCW 61, and RCW 62 at 2.4 kpc, the other associated with NGC 3576 at 3.3 kpc. The main evidence for this partition is the possibly larger distance to NGC 3576. However, given the uncertainty in this distance, which is of order 25%, we consider the one-cloud–complex picture more plausible. Further, a composite spectrum of each of the two cloud components shows that their velocities are nearly identical: -25.1 km s^{-1} *versus* -24.9 km s^{-1}. Either interpretation of this complex fits nicely within the large-scale structure of the Carina arm which we postulate.

21. $l = 294°0, b = -0°9, v = 32$ km s^{-1}.—This cloud's kinematic distance is single-valued and places it beyond the solar circle. It does not appear to have any associated objects, except possibly the supernova remnant G293.8+0.6 at 9.6 kpc (Milne 1979). The projected separation between the cloud and the SNR, at the kinematic distance of 10.7 kpc, however, is ~ 90 pc, so the relationship is clearly subject to doubt.

22. $l = 294°4, b = -0°7, v = -3$ km s^{-1}.—This cloud does not appear to have any associated optical or radio objects. Its proximity to the galactic plane and the radius–line-width relation imply it is at the far kinematic distance.

23. $l = 295°1, b = -0°8, v = 26$ km s^{-1}.—This object has four velocity components which appear disconnected in the integrated l, v map, making its classification as a single cloud complex somewhat questionable. The individual l, v maps at $b = -0°625$ and $-0°75$ (not shown here), however, show that all the emission near 295°25, from ~ 20 to 40 km s^{-1}, is connected. The spatial appearance is that of a distinct peak, resembling many of the other distant objects in the survey. The H II region G295.2-0.6 observed almost exactly in the direction of the center of the molecular cloud has an H109α recombination line velocity of 51.1 km s^{-1} (Wilson *et al.* 1970), ~ 15 km s^{-1} higher than the cloud's highest velocity component. Although the four CO components and the H II region may be unrelated, their occurrence along the same line of sight does suggest a physical connection; one wonders whether the large velocity width is the result of past star formation (i.e., supernovae and OB winds). A closer example of a molecular cloud complex with multiple velocity components along the line of sight is that associated with the supernova remnant W44 in the first quadrant. The large velocity width of this complex, ~ 40 km s^{-1}, may be due in part to interaction with the W44 supernova remnant and others no longer visible (Dame 1983). The present object is plausibly similar to the W44 molecular cloud, and we therefore included it in our catalog as a single object.

24. $l = 297°4, b = -0°5, v = 22$ km s^{-1}.—A clear separation between this cloud and cloud no. 26 is difficult to establish. If all the emission in the far side of the Carina arm between 297° and 299°7 represents a single cloud complex, the projected length is ~ 500 pc (at 11 kpc), much larger than any known Galactic molecular cloud complex. In the l, v and spatial maps, 298° appears to be a reasonable dividing line, although the exact location of this boundary is somewhat arbitrary. The radio continuum (Shaver and Goss 1970) exhibits a cluster of sources between 298° and 299° (presumably associated with cloud no. 26, below) bounded fairly sharply just below 298°, lending support to our partition. The possible physical connection of the emission between 297° and 298° at velocities greater than ~ 10 km s^{-1} is discussed in Grabelsky (1985). This cloud was assigned its kinematic distance.

The supernova remnant G296.8-0.2 at 8.7 kpc (Milne 1979) appears near the edge of the molecular cloud and may be associated. At the cloud's assumed distance of 11 kpc, the projected separation from the SNR is ~ 50 pc. No other associated objects are apparent.

25. $l = 298°6, b = 0°1, v = -35$ km s^{-1}.—This feature may be a blend of several clouds; no associated objects aid the placement or identification of possibly separate components. Its kinematic distance was adopted, placing it near the subcentral point, although this distance should be regarded as tentative since the cloud appears on the high-velocity ridge in the l, v diagram. The only major cloud between 280° and 300° that appears not to lie in the Carina arm, it may represent part of a real feature interior to the arm, such as a spur (e.g., as discussed by Humphreys 1976). Alternatively, the distance adopted may simply be too large: optical distances used for two other major clouds (no. 11 and no. 20) in the near side of the Carina arm are smaller than the kinematic distances to these objects. Humphreys (1970) reported evidence for streaming motions in the radial velocities of supergiants in the Carina arm and computed velocity corrections as a function of longitude for the stars. Applying these corrections to clouds no. 11 and no. 20 brings their kinematic and optical distances into agreement. A similar correction could be applied to cloud no. 25 but seems unwarranted without a more systematic comparison of stellar and molecular cloud velocities.

26. $l = 298°8, b = -0°2, v = 25$ km s^{-1}.—This complex, consisting of three spatial components between 298° and 300° in the far side of the arm (see Fig. 2c; Paper I, Fig. 7c), was assigned its kinematic distance of 11.9 kpc. Evidently, it is the site of very active star formation, indicated by the clustering of distant H II regions and supernova remnants observed in its direction. One H II region, G298.2-0.3, has the highest 1–20 μm luminosity of any known Galactic H II region (Frogel and Persson 1974); Lacy, Beck, and Geballe (1982) estimate that four O5.5 V stars are required to provide the ionizing radiation. Its H109α recombination line velocity is 30.6 km s^{-1} (Wilson *et al.* 1970), in agreement with the nearby molecular cloud component. G298.9-0.4, another H II region, has a radial velocity of 24.2 km s^{-1} (Wilson *et al.* 1970), also in agreement with the closest component of the complex. A third H109α

source, G298.8−0.3 ($v = 25.0$ km s^{-1}), also associated with the molecular cloud complex, may be part of G298.9−0.4 (Wilson *et al.* 1970).

Three supernova remnants are also near the line of sight to this cloud complex: G298.5−0.3, 298.6+0.0, and 299.0+0.2 at distances 16.1, 17.2, and 10.6 kpc, respectively (Milne 1979). Assuming uncertainties of 30% in the distances to these SNRs, it is possible that all three are related to the molecular cloud complex.

27. $l = 299°4, b = −0°1, v = −6$ km s^{-1}.—The far kinematic distance (9.4 kpc) for this cloud was assigned on the basis of the radius–line-width relation. A closer distance (but not the near kinematic distance) of 2.3–3.5 kpc is possible if a small Hα source at (299°9, 0°4) is associated with the cloud. Georgelin and Georgelin (1970*b*) give an optical distance of 2.3 kpc and an Hα velocity of about −10 km s^{-1} for this source, but its distance was subsequently revised to 3.5 kpc (Georgelin 1975) and the source is not included in a list of measured Hα velocities (Table V in Georgelin 1975). The evidence for an association of the Hα source with the molecular cloud is therefore not compelling.

28. $l = 300°3, b = −0°2, v = 31$ km s^{-1}.—This giant molecular cloud is apparently associated with the H II region G300.479−0.192, which has a hydrogen radio recombination line velocity (average of H109α and H110α) of 26 km s^{-1} (Caswell and Haynes 1987, hereafter CH). Formaldehyde absorption at 8 and 26 km s^{-1} is also seen toward the radio source (CH). The lower velocity absorption line is the stronger of the two and is associated with cloud no. 29; the higher velocity line presumably arises in the present giant molecular cloud (no. 28). The H II region may then be either on the far side of cloud no. 28 or on the near side but embedded in a shroud of molecular gas.

29. $l = 300°6, b = −0°2, v = 10$ km s^{-1}.—This giant molecular cloud is evidently associated with formaldehyde absorption at 8 km s^{-1} (CH) noted above (cloud no. 28).

30. $l = 301°8, b = 0°0, v = 24$ km s^{-1}.—No objects appear to be associated with this giant molecular cloud. It is fairly distinct in the spatial map (Fig. 2*d*), but blends in with cloud no. 31 in the *l, v* map.

31. $l = 302°3, b = −0°7, v = 32$ km s^{-1}.—This giant molecular cloud appears to be associated with the H II region G302.504−0.749 which has a recombination line velocity of 31 km s^{-1} (CH).

32. $l = 303°9, b = −0°4, v = 29$ km s^{-1}.—Four components can be resolved in this large cloud complex. It appears to be associated with two H II regions, G303.115−0.947 near the edge of the complex and G303.500−0.700 observed toward one of the CO peaks in the complex. The respective velocities of the H II regions are 26 and 32 km s^{-1} (CH).

33. $l = 306°9, b = −0°5, v = 25$ km s^{-1}.—This cloud is fairly distinct in both the *l, v* and spatial maps. It does not appear to have any associated objects.

34. $l = 308°0, b = −0°7, v = 32$ km s^{-1}.—This giant molecular cloud can be resolved into three spatial and velocity components but does not appear to have any associated objects.

35. $l = 311°3, b = −0°3, v = 27$ km s^{-1}.—Several components make up this large object. Although some may be unrelated, their individual kinematic distances place them all within a volume typical of largest cloud complexes, and as a group they follow the same general pattern of regular spacing along the Carina as the other large molecular objects in the survey. We therefore classified this object as a single cloud complex. Three H II regions identified by CH are evidently associated with this complex: G310.796−0.408 at 31 km s^{-1}, G311.114−0.270 at 36 km s^{-1}, and G311.619−0.599 at 32 km s^{-1}.

36. $l = 313°2, b = −0°3, v = 42$ km s^{-1}.—No associated objects are found for this giant molecular cloud. It is a distinct feature in the *l, v* and spatial maps.

37. $l = 314°0, b = −0°1, v = 28$ km s^{-1}.—This is a distinct feature in the *l, v* map; in the spatial map it shares the lowest contour with cloud no. 36. Although apparently weak, it has mass of $4.2 \times 10^5 M_\odot$. No associated objects are found.

38. $l = 315°3, b = −0°3, v = 14$ km s^{-1}.—The H II region G315.312−0.273 at 16 km s^{-1} (CH) is observed toward the central peak of this giant molecular cloud and is presumably associated. The molecular cloud is quite distinct in the *l, v* and spatial maps.

39. $l = 318°0, b = −0°3, v = 30$ km s^{-1}.—This giant cloud consists of two fairly strong components with a more diffuse background. It is evidently associated with the H II region G318.058−0.459 which has a recombination line velocity of 37 km s^{-1} (CH).

40. $l = 320°5, b = −0°5, v = 26$ km s^{-1}.—No associated objects are found for this cloud. Its appearance is similar to cloud no. 39, with two peaks and a diffuse background.

41. $l = 325°3, b = −0°1, v = 28$ km s^{-1}.—This object has two components. It is evidently associated with the H II region G324.954−0.584 at 24 km s^{-1} (CH).

42. $l = 328°5, b = −0°1, v = 30$ km s^{-1}.—No associated objects are found for this giant molecular cloud. It is distinct in the *l, v* and spatial maps. Like cloud no. 37, it is not a very strong feature in the survey but is fairly massive: $5.6 \times 10^5 M_\odot$. Lying more than 20 kpc from the Sun, it illustrates well the ability of the Chile telescope to detect these massive, CO-luminous objects at great distance.

43. $l = 335°5, b = −0°5, v = 27$ km s^{-1}.—Although this object may be less massive than $10^5 M_\odot$, we included it in our catalog because it appears to be the most distant molecular cloud detected in the Carina arm. Its apparent CO luminosity is below the nominal threshold for detection in our survey, so we did not extend the maps here and in Paper I far enough in longitude (beyond 330°) to display this cloud. However, a few long integrations with high signal-to-noise ratio in the vicinity of this cloud verify that it is real but unresolved (Bronfman, private communication). The radius given for this cloud in Table 1, since it is smaller than one beamwidth, should be regarded as an upper limit.

REFERENCES

Allen, C. W. 1973, *Astrophysical Quantities* (London: Anthlone).
Balick, B., Boeshaar, G. O., and Tull, T. R. 1980, *Ap. J.*, 242, 584.
Bigay, J. H., Garnier, R., Georgelin, Y. P., and Georgelin, Y. M. 1972, *Astr. Ap.*, 18, 301.
Blaauw, A. 1964, *Ann. Rev. Astr. Ap.*, 2, 213.
Blitz, L., and Thaddeus, P. 1980, *Ap. J. (Letters)*, 226, L39.
Bloemen, J. B. G. M., *et al.* 1986, *Astr. Ap.*, 154, 25.
Bok, B. 1937, *The Distribution of Stars in Space* (Chicago: University of Chicago Press).
Bronfman, L. 1986, Ph.D. thesis, Columbia University.

Bronfman, L., Cohen, R. S., Alvarez, H., May, J., and Thaddeus, P. 1987, *Ap. J.*, **324**, 248.

Caswell, J. L., and Haynes, R. F. 1987, *Astr. Ap.*, **171**, 261 (CH).

Claria, J. J. 1977, *Astr. Ap. Suppl.*, **27**, 145.

Cohen, R. S., Cong, H., Dame, T. M., and Thaddeus, P. 1980, *Ap. J. (Letters)*, **239**, L53.

Cohen, R. S., Grabelsky, D. A., May, J., Bronfman, L., Alvarez, H., and Thaddeus, P. 1985, *Ap. J. (Letters)*, **290**, L15.

Dame, T. M. 1983, Ph.D. dissertation, Columbia University.

Dame, T. M., Cohen, R. S., Elmegreen, B. G., and Thaddeus, P. 1986, *Ap. J.*, **305**, 892.

Dickel, J. R. 1973, *Ap. Letters*, **15**, 61.

Elliot, K. H., and Malin, D. F. 1979, *M.N.R.A.S.*, **186**, 45P.

Elmegreen, B. G. 1987, *Ap. J.*, **312**, 626.

Elmegreen, B. G., and Lada, C. J. 1976, *Ap. J.*, **81**, 1089.

Feinstein, A., Marraco, H. G., and Forte, J. C. 1976, *Astr. Ap. Suppl.*, **24**, 389.

Feinstein, A., Marraco, H. G., and Muzzio, J. C. 1973, *Astr. Ap. Suppl.*, **12**, 331.

Frogel, J. A., and Persson, S. E. 1974, *Ap. J.*, **192**, 351.

Frogel, J. A., Persson, S. E., and Aaronson, M. 1977, *Ap. J.*, **213**, 723.

Georgelin, Y. 1975, Ph.D. dissertation, Universite de Provence, Observatoire de Marseille.

Georgelin, Y. M., and Georgelin, Y. P. 1976, *Astr. Ap.*, **49**, 57.

Georgelin, Y. M., Lortet, M. C., and Testor, G. 1986, *Astr. Ap.*, **162**, 265.

Georgelin, Y. P., and Georgelin, Y. M. 1970a, *Astr. Ap.*, **6**, 349.

———. 1970b, *Astr. Ap.*, **7**, 133.

Goss, W. M., Manchester, R. N., Brooks, J. W., Sinclair, M. W., Manefield, G., and Danziger, I. J. 1980, *M.N.R.A.S.*, **191**, 533.

Goss, W. M., and Radhakrishnan, V. 1969, *Ap. Letters*, **4**, 199.

Goss, W. M., Radhakrishnan, V., Brooks, J. W., and Murray, J. D. 1972, *Ap. J. Suppl.*, **24**, 123.

Goss, W. M., and Shaver, P. A. 1970, *Australian J. Phys. Ap. Suppl.*, **14**, 1.

Goy, G. 1973, *Astr. Ap. Suppl.*, **12**, 277.

Grabelsky, D. A. 1985, Ph.D. thesis, Columbia University.

Grabelsky, D. A., Cohen, R. S., Bronfman, L., Thaddeus, P., and May, J. 1987, *Ap. J.*, **315**, 122 (Paper I).

Grabelsky, D. A., Cohen, R. S., and Thaddeus, P. 1986, in *Star Formation in Galaxies*, ed. C. J. Persson (Washington: GPO), p. 67.

Gum, C. S. 1955, *Mem. R.A.S.*, **67**, 155.

Henderson, A. P., Jackson, P. D., and Kerr, F. J. 1982, *Ap. J.*, **263**, 116.

Hoffleit, D. 1953, *Harvard Ann.*, **119**, 37.

Humphreys, R. M. 1970, *A.J.*, **75**, 602.

———. 1972, *Astr. Ap., J.*, **20**, 29.

Humphreys, R. M. 1976, *Pub. A.S.P.*, **58**, 647.

———. 1978, *Ap. J. Suppl.*, **38**, 309.

Kerr, F. J. 1970, in *IAU Symposium 38, The Spiral Structure of our Galaxy*, ed. W. Becker and G. Contopoulos (Dordrecht: Reidel), p. 95.

Kerr, F. J., and Kerr, M. 1970, *Ap. Letters*, **6**, 175.

Kerr, F. J., and Lynden-Bell, D. 1986, *M.N.R.A.S.*, **221**, 1023.

Kirshner, R. P., and Winkler, F. P., Jr. 1979, *Ap. J.*, **227**, 853.

Kutner, M. L., Tucker, K. D., Chin, G., and Thaddeus, P. 1977, *Ap. J.*, **215**, 521.

Lacy, J. H., Beck, S. C., and Geballe, T. R. 1982, *Ap. J.*, **255**, 510.

Lada, C. J., Elmegreen, B. G., Cong, H.-I., and Thaddeus, P. 1978, *Ap. J. (Letters)*, **225**, L39.

Lebrun, F., *et al.* 1983, *Ap. J.*, **274**, 231.

Liszt, H. S., and Burton, W. B. 1981, *Ap. J.*, **243**, 778.

Lyngå, G. 1970, *Astr. Ap.*, **8**, 41.

Milne, D. K. 1979, *Australian J. Phys.*, **32**, 83.

Milne, D. K., Wilson, T. L., Gardner, F. F., and Mezger, P. G. 1969, *Ap. Letters*, **4**, 121.

Moffat, A. F. J. 1983, *Astr. Ap.*, **124**, 273.

Moffat, A. F. J., and Vogt, N. 1975, *Astr. Ap. Suppl.*, **20**, 125.

Morgan, W. W., Sharpless, S., and Osterbrock, D. E. 1952, *A.J.*, **57**, 3.

Morgan, W. W., Whitford, A. E., and Code, A. D. 1953, *Ap. J.*, **118**, 318.

Sanders, D. B., Solomon, P. M., and Scoville, N. Z. 1984, *Ap. J.*, **276**, 182.

Sandqvist, A. 1977, *Astr. Ap.*, **57**, 467.

Schwartz, P. R., Wilson, W. J., and Epstein, E. E. 1973, *Ap. J.*, **186**, 529.

Shaver, P. A., and Goss, W. M. 1970, *Australian J. Phys.*, **14**, 77.

Simonson, S. C., III. 1970, *Astr. Ap.*, **9**, 163.

Solomon, P. M., Sanders, D. B., and Scoville, N. Z. 1979, in *IAU Symposium 84, The Large-Scale Characteristics of the Galaxy*, ed. W. B. Burton (Dordrecht: Reidel), p. 35.

Stothers, R. 1972, *Ap. J.*, **175**, 431.

Tucker, K. D., Kutner, M. L., and Thaddeus, P. 1973, *Ap. J. (Letters)*, **186**, L13.

Turner, D. G. 1978, *A.J.*, **83**, 1081.

Turner, D. G., Grieve, G. R., Herbst, W., and Harris, W. E. 1980, *A.J.*, **85**, 1193.

van den Bergh, S. 1978, *Astr. Ap.*, **63**, 275.

Vogt, N., and Moffat, A. F. J. 1975, *Astr. Ap.*, **39**, 477.

Walborn, N. R. 1971, *Ap. J. (Letters)*, **167**, L31.

———. 1973, *Ap. J.*, **179**, 517.

———. 1973, *Ap. J. (Letters)*, **182**, L21.

Weaver, H. 1970, in *IAU Symposium 38, The Spiral Structure of our Galaxy*, ed. W. Becker and G. Contopoulos (Dordrecht: Reidel), p. 126.

Wilson, T. L., Mezger, P. G., Gardner, F. F., and Milne, D. K. 1970, *Astr. Ap.*, **6**, 364.

L. BRONFMAN: Departmento de Astronomia, Universidad de Chile, Casilla 36-D, Santiago, Chile

R. S. COHEN: 51 Seventh Avenue, Brooklyn, NY   11217

D. A. GRABELSKY: Northwestern University, Department of Physics and Astronomy, Evanston, IL   60201

P. THADDEUS: Harvard-Smithsonian Center for Astrophysics, 60 Garden Street, Cambridge, MA   02138